

# Intergalactic Magnetic Field and Arrival Direction of Ultra-High-Energy Protons

Dongsu Ryu<sup>1,4</sup>, Santabrata Das<sup>2</sup>, and Hyesung Kang<sup>3</sup>

## ABSTRACT

We studied how the intergalactic magnetic field (IGMF) affects the propagation of super-GZK protons that originate from extragalactic sources within the local GZK sphere. Toward this end, we set up hypothetical sources of ultra-high-energy cosmic-rays (UHECRs), virtual observers, and the magnetized cosmic web in a model universe constructed from cosmological structure formation simulations. We then arranged a set of reference objects mimicking active galactic nuclei (AGNs) in the local universe, with which correlations of simulated UHECR events are analyzed. With our model IGMF, the deflection angle between the arrival direction of super-GZK protons and the sky position of their actual sources is quite large with the mean value of  $\langle\theta\rangle \sim 15^\circ$  and the median value of  $\tilde{\theta} \sim 7 - 10^\circ$ . On the other hand, the separation angle between the arrival direction and the sky position of nearest reference objects is substantially smaller with  $\langle S \rangle \sim 3.5 - 4^\circ$ , which is similar to the mean angular distance in the sky to nearest neighbors among the reference objects. This is a direct consequence of our model that the sources, observers, reference objects, and the IGMF all trace the matter distribution of the universe. The result implies that extragalactic objects lying closest to the arrival direction of UHECRs are not necessary their actual sources. With our model for the distribution of reference objects, the fraction of super-GZK proton events, whose closest AGNs are true sources, is less than 1/3. We discussed implications of our findings for correlation studies of real UHECR events.

---

<sup>1</sup>Department of Astronomy and Space Science, Chungnam National University, Daejeon 305-764, Korea; ryu@canopus.cnu.ac.kr

<sup>2</sup>Department of Physics, Indian Institute of Technology Guwahati, Guwahati, 781039, Assam, India; sbdas@iitg.ernet.in

<sup>3</sup>Department of Earth Sciences, Pusan National University, Pusan 609-735, Korea; kang@uju.es.pusan.ac.kr

<sup>4</sup>Corresponding Author

*Subject headings:* cosmic rays — large-scale structure of universe — magnetic fields — method: numerical

## 1. Introduction

The nature and origin of ultra-high-energy cosmic rays (UHECRs), especially above the so-called Greisen-Zatsepin-Kuz'min (GZK) energy of  $E_{\text{GZK}} \approx 50$  EeV ( $1 \text{ EeV} = 10^{18} \text{ eV}$ ), has been one of most perplexing puzzles in astrophysics over five decades and still remains to be understood (see Nagano & Watson 2000, for a review). The highest energy CR detected so far is the Fly's Eye event with an estimated energy of  $\sim 300$  EeV (Bird et al. 1994). At these high energies protons and nuclei cannot be confined and accelerated effectively within our Galaxy, so the sources of UHECRs are likely to be extragalactic.

At energies higher than  $E_{\text{GZK}}$ , it is expected that protons lose energy and nuclei are photo-disintegrated via the interactions with the cosmic microwave background radiation (CMB) along their trajectories in the intergalactic space (Greisen 1966; Zatsepin & Kuz'min 1966; Puget et al. 1976). The former is known as the GZK effect. So a significant suppression in the energy spectrum above  $E_{\text{GZK}}$  could be regarded as an observational evidence for the extragalactic origin of UHECRs (see, e.g., Berezhinsky et al. 2006). However, the accurate measurement of the UHECR spectrum is very difficult, partly because of extremely low flux of UHECRs. But a more serious hurdle is the uncertainties in the energy calibration inherent in detecting and modeling extensive airshower events (e.g., Nagano & Watson 2000; Watson 2006). Nevertheless, both the Yakutsk Extensive Air Shower Array (Yakutsk) and the High Resolution Fly's Eyes (HiRes) reported observations of the GZK suppression (Egorova et al. 2004; Abbasi et al. 2008a), while the Akeno Giant Air Shower Array (AGASA) claimed a conflicting finding of no suppression (Shinozaki & Teshima 2004). More recent data from the Pierre Auger Observatory (Auger) support the existence of the GZK suppression (Abraham et al. 2008b; Schüssler et al. 2009). Below  $E_{\text{GZK}}$ , however, the four experiments reported the fluxes that are different from each other by up to a factor of several, implying the possible existence of systematic errors in their energy calibrations (Berezhinsky 2009).

The overall sky distribution of the arrival directions of UHECRs below  $E_{\text{GZK}}$  seems to support the isotropy hypothesis (see, e.g., Nagano & Watson 2000). This is consistent with the expectation of uniform distribution of extragalactic sources; the interaction length (i.e. horizon distance) of protons below  $E_{\text{GZK}}$  is a few Gpc and the universe can be considered homogeneous and isotropic on such a large scale. The horizon distance for super-GZK events, however, decreases sharply with energy and  $R_{\text{GZK}} \sim 100$  Mpc for  $E = 100\text{EeV}$

(Berezinsky & Grigor’eva 1988). The matter distribution inside the local GZK horizon ( $R_{\text{GZK}}$ ) is inhomogeneous. Since powerful astronomical objects are likely to form at deep gravitational potential wells, we expect the distribution of the UHECR sources would be inhomogeneous as well. Hence, if super-GZK proton events point their sources, their arrival directions should be anisotropic.

The anisotropy of super-GZK events, hence, has been regarded to provide an important clue that unveils the sources of UHECRs. So far, however, the claims derived from analyses of different experiments are often tantalizing and sometimes conflicting. For instance, with an excessive number of pairs and one triplet in the arrival direction of CRs above 40 EeV, the AGASA data support the existence of small scale clustering (Hayashida et al. 1996; Takeda et al. 1999). On the other hand, the HiRes stereo data are consistent with the hypothesis of null clustering (Abbasi et al. 2004, 2009). The auto-correlation analysis of the Auger data reported a weak excess of pairs for  $E > 57$  EeV (Abraham et al. 2008a). In addition, the Auger Collaboration found a correlation between highest energy events and the large scale structure (LSS) of the universe using nearby active galactic nuclei (AGNs) in the Véron-Cetty & Véron (2006) catalog (The Pierre Auger Collaboration 2007; Abraham et al. 2008a; Hague et al. 2009) as well as using nearby objects in different catalogs (Aublin et al. 2009). A correlation between highest AGASA events with nearby galaxies from SDSS was reported (Takami et al. 2009). The HiRes data, however, do not show such correlation of highest energy events with nearby AGNs (Abbasi et al. 2008b), but instead show a correlation with distant BL Lac objects (Abbasi et al. 2006).

The interpretation of anisotropy and correlation analyses is, however, complicated owing to the intervening galactic magnetic field (GMF) and intergalactic magnetic field (IGMF); the trajectories of UHECRs are deflected by the magnetic fields as they propagate through the space between sources and us, and hence, their arrival directions are altered. Even with considerable observational and theoretical efforts, however, the nature of the GMF and the IGMF is still poorly constrained. Yet, models for the GMF generally assume a strength of  $\sim$  a few  $\mu\text{G}$  and a coherence length of  $\sim 1$  kpc for the field in the Galactic halo (see, e.g., Stanev 1997), and predict the deflection of UHE protons due to the GMF to be  $\theta \sim$  a few degrees (see, e.g., Takami & Sato 2008). The situation for the IGMF in the LSS has been confusing. Adopting a model for the IGMF with the average strength of  $\langle B \rangle \sim 100$  nG in filaments, Sigl et al. (2003) showed that the deflection of UHECRs due to the IGMF could be very large, e.g.,  $\theta > 20^\circ$  for protons above 100 EeV. On the other hand, Dolag et al. (2005) adopted a model with  $\langle B \rangle \sim 0.1$  nG in filaments and showed that the deflection should be negligible, e.g.,  $\theta \ll 1^\circ$  for protons with 100 EeV.

Recently, Ryu et al. (2008) proposed a physically motivated model for the IGMF, in

which a part of the gravitational energy released during structure formation is transferred to the magnetic field energy as a result of the turbulent dynamo amplification of weak seed fields in the LSS of the universe. In the model, the IGMF follows largely the matter distribution in the cosmic web, and the strength and coherence length are predicted to be  $\langle B \rangle \sim 10$  nG and  $\sim 1$  Mpc for the field in filaments. Such field in filaments is expected to induce the Faraday rotation (Cho & Ryu 2009), which is consistent with observation (Xu et al. 2006). With this model IGMF, Das et al. (2008) (Paper I hereafter) calculated the trajectories of UHE protons ( $E > 10$  EeV) that were injected at extragalactic sources associated with the LSS in a simulated model universe. We then estimated that only  $\sim 35$  % of UHE protons above 60 EeV would arrive at us with  $\theta \leq 5^\circ$  and the average value of deflection angle would be  $\langle \theta \rangle \sim 15^\circ$ . Note that the deflection angle of  $\langle \theta \rangle \sim 15^\circ$  is much larger than the angular window of  $3.1^\circ$  used by the Auger collaboration in the study of the correlation between highest energy UHECR events and nearby AGNs (The Pierre Auger Collaboration 2007; Abraham et al. 2008a; Hague et al. 2009).

In this contribution, as a follow-up work of Paper I, we investigate the effects of the IGMF on the arrival direction of super-GZK protons above 60 EeV coming from sources within 75 Mpc. The limiting parameters for energy and source distance are chosen to match the recent analysis of the Auger collaboration. Without knowing the true sources of UHECRs, the statistics that can be obtained with observational data from experiments are limited; some statistics that are essential to reveal the nature of sources are difficult or even impossible to be constructed. On the other hand, with data from simulations, any statistics can be explored. In that sense, simulations complement experiments. Here, with the IGMF suggested by Ryu et al. (2008), we argue that the large deflection angle of super-GZK protons due to the IGMF is not inconsistent with the anisotropy and correlation recently reported by the Auger collaboration. However, the large deflection angle implies that the nearest object to a UHECR event in the sky is not necessarily its actual source. In Section 2, we describe our models for the LSS of the universe, IGMF, observers, and sources of UHECRs, reference objects for correlation study, and simulations. In Section 3, we present the results, followed by a summary and discussion in Section 4.

## 2. Models and Simulations

In our study, the following elements are necessary: 1) a model for the IGMF on the LSS, 2) a set of virtual observers that represent “us”, an observer at the Earth, in a statistical way, 3) a set of hypothetical sources of UHE protons with a specified injection spectrum, and 4) a set of reference objects with which we performed a correlation study of simulated

events. In Paper I, we described in detail how we set up 1), 2), and 3) by using data from cosmological structure formation simulations. Below, we briefly summarize models for 1), 2), and 3) and explain in details the reason to introduce “reference objects” in this study.

## 2.1. Large Scale Structure of the Universe

We assumed a concordance  $\Lambda$ CDM model with the following parameters:  $\Omega_{\text{BM}} = 0.043$ ,  $\Omega_{\text{DM}} = 0.227$ , and  $\Omega_{\Lambda} = 0.73$ ,  $h \equiv H_0/(100 \text{ km/s/Mpc}) = 0.7$ , and  $\sigma_8 = 0.8$ . The model universe for the LSS was generated through simulations in a cubic region of comoving size  $100h^{-1}(\equiv 143)$  Mpc with  $512^3$  grid zones for gas and gravity and  $256^3$  particles for dark matter, using a PM/Eulerian hydrodynamic cosmology code described in Ryu et al. (1993). The simulations have a uniform spatial resolution of  $195.3h^{-1}$  kpc. The standard set of gasdynamic variables, the gas density,  $\rho_g$ , temperature,  $T$ , and the flow velocity,  $\mathbf{v}$ , were used to calculate the quantities required in our model such as the X-ray emission weighted temperature  $T_X$ , the vorticity,  $\omega$ , and the turbulent energy density,  $\varepsilon_{\text{turb}}$ , at each grid.

## 2.2. Intergalactic Magnetic Field

We adopted the IGMF from the model by Ryu et al. (2008); the model proposes that turbulent-flow motions are induced via the cascade of the vorticity generated at cosmological shocks during the formation of the LSS of the universe, and the IGMF is produced as a consequence of the amplification of weak seed fields of any origin by the turbulence. Then, the energy density (or the strength) of the IGMF can be estimated with the eddy turnover number and the turbulent energy density as follow:

$$\varepsilon_B = \phi \left( \frac{t}{t_{\text{eddy}}} \right) \varepsilon_{\text{turb}}. \quad (1)$$

Here, the eddy turnover time is defined as the reciprocal of the vorticity at driving scales,  $t_{\text{eddy}} \equiv 1/\omega_{\text{driving}}$  ( $\omega \equiv \nabla \times \mathbf{v}$ ), and  $\phi$  is the conversion factor from turbulent to magnetic energy that depends on the eddy turnover number  $t/t_{\text{eddy}}$ . The eddy turnover number was estimated as the age of universe times the magnitude of the local vorticity, that is,  $t_{\text{age}} \omega$ . The local vorticity and turbulent energy density were calculated from cosmological simulations for structure formation described above. A functional form for the conversion factor was derived from a separate, incompressible, magnetohydrodynamic (MHD) simulation of turbulence dynamo.

For the direction of the IGMF, we used that of the passive fields from cosmological

simulations, in which magnetic fields were generated through the Biermann battery mechanism (Biermann 1950) at cosmological shocks and evolved passively along with flow motions (Kulsrud et al. 1997; Ryu et al. 1998). In principle, if we had performed full MHD simulations, we could have followed the amplification of the IGMF through turbulence dynamo. In practice, however, the currently available computational resources do not allow a numerical resolution high enough to reproduce the full development of MHD turbulence. Since the numerical resistivity is larger than the physical resistivity by many orders of magnitude, the growth of magnetic fields is saturated before dynamo action becomes fully operative (see, e.g., Kulsrud et al. 1997). This is the reason why we adopted the model of Ryu et al. (2008) to estimate the strength of the IGMF, but we still used the the passive fields from cosmological simulations to model the field direction.

Figure 1 shows the distribution of magnetic field strength in a slice of  $(143 \text{ Mpc})^2$  in our model universe. It shows that the IGMF is structured like the matter in the cosmic web. As a matter of fact, the distribution of the IGMF is very well correlated with that of matter. The strongest magnetic field of  $B \gtrsim 0.1 \mu\text{G}$  is found in and around clusters, while the field is weaker in filaments, sheets, and voids. In filaments which are mostly composed of the warm-hot intergalactic medium (WHIM) with  $T = 10^5 - 10^7 \text{ K}$ , the IGMF has  $\langle B \rangle \sim 10 \text{ nG}$  and  $\langle B^2 \rangle^{1/2} \sim \text{a few} \times 10 \text{ nG}$  (Ryu et al. 2008). Note that the deflection of UHECRs arises mostly due to the field in filaments (see Paper I). The energy density of the IGMF in filaments is  $\varepsilon_B \sim 10^{-16} \text{ ergs cm}^{-3}$ , which is a few times smaller than the gas thermal energy density and an order of magnitude smaller than the gas kinetic energy density there.<sup>1</sup> The IGMF in filaments induces the Faraday rotation; the root-mean-square (rms) value of rotation measure (RM) is predicted to be a few  $\text{rad m}^{-1}$  (Cho & Ryu 2009). That is consistent with the values of RM toward the Hercules and Perseus-Pisces superclusters reported in Xu et al. (2006).<sup>2</sup>

### 2.3. Observer Locations

In the study of the arrival direction of UHECRs, the IGMF around us, that is, in the Local Group, is important too. It would have been ideal to place “the observer” where the

---

<sup>1</sup>We note that our model does not include a possible contribution to the IGMF from galactic black holes, AGN feedback (see, e.g., Kronberg et al. 2001); so our model may be regarded to provide a baseline for the IGMF. With the contribution, the real IGMF might be even stronger, resulting in even larger deflection (see Section 3.1).

<sup>2</sup>The values of  $|\text{RM}|$  in Xu et al. (2006) is an order of magnitude larger than the value above, a few  $\text{rad m}^{-1}$ . However, Xu et al. (2006) quoted the path length, which is about two orders of magnitude larger.

IGMF is similar to that in the Local group. Unfortunately, however, little is known about the IGMF in the Local Group. Hence, instead, we placed “virtual” observers based on the X-ray emission weighted temperature  $T_X$ . The groups of galaxies that have the halo temperature similar to that of the Local Group,  $0.05 \text{ keV} < kT_X < 0.5 \text{ keV}$  (Rasmussen & Pedersen 2001), were identified. About 1400 observer locations were chosen by the temperature criterion. In reality, there should be only one observer on the Earth. But in our modeling we could choose a number of observer locations to represent statistically “us” without loss of generality, since the simulated universe is only one statistical representation of the real universe. Then, we modeled observers as a sphere of radius  $0.5h^{-1} \text{ Mpc}$  located at the center of host groups, in order to reduce the computing time to a practical level. The distribution of handful observers are shown schematically in Figure 1. One can see that the observers (groups) are not distributed uniformly, but instead they are located mostly along filaments.

#### 2.4. AGNs as Reference Objects

As noted in Introduction, the Auger Collaboration recently reported a correlation between the direction of their highest energy events and the sky position of nearby AGNs from the 12th edition of the Véron-Cetty & Véron (2006) (VCV) catalog; the correlation has the maximum significance for UHECRs with  $E \gtrsim 60 \text{ EeV}$  and AGNs with distance  $D \lesssim 75 \text{ Mpc}$  (The Pierre Auger Collaboration 2007; Abraham et al. 2008a; Hague et al. 2009). There are about 450 AGNs with  $D \lesssim 75 \text{ Mpc}$  (more precisely, 442 AGNs with redshift  $z \leq 0.018$ , for which the maximum significance of the correlation was found) in the VCV catalog. In that study it is not known which subclass of those AGNs or what fraction of them are really true sources of UHECRS. Here, we regard those AGNs as “reference objects”, with which correlation studies are performed.

In order to compare our correlation study with that of the Auger collaboration, we specified the following condition to determine “model” reference objects in the simulated universe: 1) the number of the objects within 75 Mpc from each observer should be on average  $\sim 500$ , and 2) their spatial distribution should trace the LSS in a way similar to the AGN distribution in the real universe. To set up the location of such reference objects, we identified “clusters” of galaxies with  $kT_X \gtrsim 0.1 \text{ keV}$  in the simulated universe. Of course some of these clusters with  $kT_X \lesssim$  a few keV should be classified as groups of galaxies. But for simplicity we call all of them as clusters. The reason behind this selection condition is that the gas temperature is directly related with the depth of gravitational potential well; the hottest gas resides in the densest, most nonlinear regions of the LSS where the most luminous and energetic objects (e.g. AGNs) form through frequent mergers of galaxies. We

then assumed that each cluster hosts one reference object at its center. For each observer, we generated a list of reference objects inside a sphere of radius 75 Mpc, whose number is on average  $\sim 500$ ; the exact number of reference objects varies somewhat for different observers. Then, each observer has its own sky distribution of reference objects, with which we studied the correlation of simulated events. Although our reference objects could be any astronomical objects that trace the LSS, hereafter we refer them as “model AGNs”, because the selection criteria were chosen to match the number of AGNs with that from the VCV catalog. Figure 1 shows the schematic distribution of handful model AGNs at the center of host clusters. Obviously the host clusters (and the AGNs) are not uniformly distributed either.

In our set-up, the distance to the model AGNs,  $D$ , can be arbitrarily small. In reality, however, the closest AGN in the VCV catalog is NGC 404 at  $D \sim 3$  Mpc in the constellation Andromeda (Karachentsev et al. 2004). So the model AGNs with the distance from each observer  $D < D_{\min} \equiv 3$  Mpc were excluded.

We checked the angular distance  $Q$  between a given reference object to its nearest neighboring object. For a set of 442 objects (the number of the AGNs with  $z \leq 0.018$  in the VCV catalog), if they are distributed isotropically over the sky of  $4\pi$  radian, the average value of  $Q$  would be  $\langle Q_{\text{iso}} \rangle \approx 11^\circ$ . With the 442 AGNs from the VCV catalog, on the other hand,  $\langle Q_{\text{VCV}} \rangle = 3.55^\circ$ . The fact that  $\langle Q_{\text{VCV}} \rangle < \langle Q_{\text{iso}} \rangle$  means that the distribution of the AGNs from the VCV catalog is not isotropic, but highly clustered, following the matter distribution in the LSS of the universe. We note that  $\langle Q_{\text{VCV}} \rangle = 3.55^\circ$  is similar to the angular window of  $3.1^\circ$  used in the Auger study. Clearly this agreement is not accidental, but rather consequential. For the sets of  $\sim 500$  model AGNs in our simulations, the average angular distance is  $\langle Q_{\text{AGN}} \rangle = 3.68^\circ \pm 1.66^\circ$ . The error was estimated with  $\langle Q_{\text{AGN}} \rangle$  for  $\sim 1400$  observers. That fact that  $\langle Q_{\text{AGN}} \rangle \sim \langle Q_{\text{VCV}} \rangle$  indicates that the spatial clustering of our model AGNs is on average comparable to that of the AGNs from the VCV catalog. This provides a justification for our selection criteria for model AGNs in the simulated universe. We note that  $Q$  is an intrinsic property of the distribution of the reference objects in the sky and has nothing to do with UHECRs.

## 2.5. Sources of UHECRs

Although AGN is one of viable candidates that would produce UHECRs (see, e.g., Nagano & Watson 2000, for the list of viable candidates), there is no compelling reason that all the nearby AGNs are the sources of UHECRs. In this paper, we considered three models with different numbers of sources,  $N_{\text{src}}$  (see Table 1), to represent different subsets of AGNs.



1) Among AGNs, radio galaxies are considered to be the most promising sources of UHECRs (see, e.g., Biermann & Strittmatter 1987), and there are 28 known radio galaxies within  $D \leq 75$  Mpc. So in Model C, we considered on average 28 model AGNs located at 28 hottest host clusters ( $kT_x \gtrsim 0.8\text{keV}$ ) within a sphere of radius 75 Mpc as true sources of UHECRs. 2) Based on the ratio of singlet to doublet events, on the other hand, Abraham et al. (2008a) argued that the lower limit on the number of sources of UHECRs would be around 61. Following this claim, in Model B, we regarded on average 60 model AGNs located at 60 hottest host clusters ( $kT_x \gtrsim 0.55\text{keV}$ ) as true sources of UHECRs. 2) In Model A, we regarded all the model AGNs (reference objects) as true sources of UHECRs.

## 2.6. Simulations of Propagation of UHE Protons

At sources, UHE protons were injected with power-law energy spectrum;  $N_{\text{inj}}(E_{\text{inj}}) \propto E_{\text{inj}}^{-\gamma}$  for  $6 \times 10^{19} \text{ eV} \leq E_{\text{inj}} \leq 10^{21} \text{ eV}$ , where  $\gamma$  is the injection spectral index. We considered the two cases of  $\gamma = 2.7$  and  $2.4$ . At each source, protons were randomly distributed over a sphere of radius  $0.5h^{-1}$  Mpc, and then launched in random directions.

We then followed the trajectories of UHE protons in our model universe with the IGMF, by numerically integrating the equations of motion;

$$\frac{d\mathbf{r}}{dt} = \mathbf{v}, \quad \frac{d\mathbf{p}}{dt} = e(\mathbf{v} \times \mathbf{B}), \quad (2)$$

where  $\mathbf{p}$  is the momentum. During propagation UHE protons interact with the CMB, and the dominant processes for energy loss are the pion and pair productions. The energy loss was treated with the continuous-loss approximation (Berezinsky et al. 2006). The adiabatic loss due to the cosmic expansion was ignored.

Table 1. Models of different numbers of sources

Model	$N_{\text{src}}$	host clusters	$\langle\theta\rangle^{\text{a}}$	$\tilde{\theta}$	$\langle S_{\text{sim}}\rangle^{\text{a}}$	$\tilde{S}_{\text{sim}}$
A	$\sim 500$	$kT_X \gtrsim 0.1\text{keV}$	13.98	7.01	3.58	2.80
B	60	$kT_X \gtrsim 0.55\text{keV}$	15.33	8.80	3.97	3.19
C	28	$kT_X \gtrsim 0.8\text{keV}$	17.76	10.45	4.23	3.43

<sup>a</sup>Deflection angle  $\theta$  and separation angle  $S$  are defined in Section 3

We let UHE protons continue the journey, visiting several observers during flight, until the energy falls to 60 EeV. At observers, the events with  $E \geq 60$  EeV were recorded and analyzed.

### 3. Results

#### 3.1. Deflection Angle

In Paper I, we considered the deflection angle,  $\theta$ , between the arrival direction of UHECR events and the sky position of their sources (see Figure 2). Obviously this angle can be calculated only when the true sources are known, which is not the case in experiments. In the simulated universe, our model AGNs and observers are located in strongly magnetized regions. As illustrated in Figure 1, UHECRs first have to escape from magnetic halos surrounding sources, then travel through more or less void regions (path 1) or through filaments (path 2), and finally penetrate into magnetic halos around observers, to reach observers. So the degree of deflection depends not only on the magnetic field along trajectories but also on the fields at host clusters and groups of sources and observers. Since the gas temperature, the depth of gravitational potential well, and the magnetic field energy density are related as  $kT_X \propto \Phi \propto \varepsilon_B$  in our model, hotter clusters and groups would have stronger fields. So we expect that if sources and observers are located at hotter hosts,  $\theta$  would be larger on average.

Figure 3 shows  $\theta$  versus  $D_\theta$  for UHE proton events recorded at observers in our simulations. Here,  $D_\theta$  denotes the distance to the actual sources of events. The top, middle, and bottom panels are for Models A, B, and C, respectively. Only the case of injection spectral index  $\gamma = 2.7$  is presented. The case of  $\gamma = 2.4$  is similar. Each dot represents one simulated event, and there are about  $10^5$  events in each Model. The upper circles connected with dotted lines represent the mean values of  $\theta$  in the distance bins of  $[D_\theta, D_\theta + \Delta D_\theta]$ . The mean deflection angle averaged over all the simulated events is  $\langle \theta \rangle = 13.98^\circ$ ,  $15.33^\circ$ , and  $17.76^\circ$  for  $\gamma = 2.7$  in Model A, Model B, and Model C, respectively. The lower circles connected with solid lines represent the median values of  $\theta$ . The median value for all the simulated events is  $\tilde{\theta} = 7.01^\circ$ ,  $8.80^\circ$ , and  $10.45^\circ$  for  $\gamma = 2.7$  in Model A, Model B, and Model C, respectively. The values of  $\langle \theta \rangle$  and  $\tilde{\theta}$  for  $\gamma = 2.4$  are similar. The marks connected with vertical solid lines on the both sides of median values are the first and third quartiles in the distance bins, which provide a measure of the dispersion of  $\theta$ .

We note the following points. (1) With our IGMF, the mean deflection angle of UHE protons due to the IGMF is quite large, much larger than the angular window of  $3.1^\circ$  used

in the Auger correlation study. It is also much larger than the mean deflection angle that is expected to result from the Galactic magnetic field, which is a few degrees (Takami & Sato 2008). (2) The mean deflection angle is largest in Model C and smallest in Model A. Recall that in Model C sources are located only at 28 hottest clusters, while in Model A all 500 clusters include sources (see Table 1). The UHECR events from hotter clusters tend to experience more deflection, as noted above. So the mean of deflection angles in the model with hotter host clusters is larger. (3) The mean value of  $\theta$  has a minimum at  $D_{\theta,\min} \sim 20\text{--}30$  Mpc, which compares to a typical length of filaments. As we pointed out in Paper I, this is a consequence of the structured magnetic fields that are concentrated along filaments and at clusters. In an event with  $D_\theta < D_{\theta,\min}$ , the source and observer are more likely to belong to the same filament, and so the particle is more likely to travel through strongly magnetized regions and suffer large deflection (see the path 2 in Figure 1). In the opposite regime, the source and observer are likely to belong to different filaments, so the particle would travel through void regions (see the path 1 in Figure 1). (4) For the events with  $D_\theta > D_{\theta,\min}$ , the mean and dispersion of  $\theta$  increase with  $D_\theta$ . Such trend is expected, since in the diffusive transport model of the propagation of UHECRs, the deflection angle increases with distance as  $\theta_{\text{rms}} \propto \sqrt{D_\theta}$  (see, e.g., Kotera & Lemoine 2009, and references therein). (5) There are more events from nearby sources than from distant sources, although all the sources inject the same number of UHECRs in our model. The smaller number of events for larger  $D_\theta$  should be mostly a consequence of energy loss due to the interaction with the CMB.

### 3.2. Separation Angles

In this study, we also consider the separation angle,  $S$ , between the arrival direction of UHECR events and the sky position of nearest reference objects (see Figure 2). The angle can be calculated with observation data, once a class of reference objects (e.g. AGNs, galaxies gamma-ray bursts, and etc.) is specified. For example, The Pierre Auger Collaboration (2007) took the AGNs within 75 Mpc in the VCV catalog as the reference objects for their correlation study. However, for a given UHECR event, the nearest AGN in the sky may not be the actual source; hence, the separation angle between a UHECR event and its nearest AGN is not necessarily the same as the deflection angle of the event (Hillas 2009; Ryu et al. 2009).

We obtained  $S$  for simulated events with our model reference objects (AGNs). Figure 4 shows  $S$  versus  $D_S$ . Here,  $D_S$  denotes the distance to nearest AGNs. Again only the case of  $\gamma = 2.7$  is presented, and the case of  $\gamma = 2.4$  is similar (see Figure 5). The circles connected with solid line represent the mean values of  $S$  for the events with nearest AGNs

in the distance bins of  $[D_S, D_S + \Delta D_S]$ . The mean separation angle averaged over all the simulated events is  $\langle S_{\text{sim}} \rangle = 3.58^\circ$ ,  $3.97^\circ$ , and  $4.23^\circ$  for  $\gamma = 2.7$  in Models A, B, and C, respectively.

We note the following points. (1) The mean separation angle is much smaller than the mean deflection angle,  $\langle S_{\text{sim}} \rangle \sim (1/4)\langle \theta \rangle$  (see the next section for further discussion). (2) The mean separation angle is largest in Model C and smallest in Model A, although the difference of  $\langle S_{\text{sim}} \rangle$  among the models is less than that of  $\langle \theta \rangle$ . With larger deflection angles in Model C, there is a higher probability for a event to be found further away from the region where model AGNs are clustered, so  $S$  is on average larger as well. (3) Similarly as in the  $\theta$  versus  $D_\theta$  distribution, the distribution of  $\langle S_{\text{sim}} \rangle$  has the minimum at around  $D_S \sim 35$  Mpc. This is again a signature of the filamentary structures of the LSS. (4) Contrary to  $D_\theta$ , there are more events with larger  $D_S$  than with smaller  $D_S$ . It is simply because there are more AGNs with larger  $D_S$ .

### 3.3. Comparison with the Auger Data

We also obtained  $S$  for the 27 Auger events of highest energies, published in Abraham et al. (2008a), with 442 nearby AGNs from the VC catalog. In Figure 5, we compare the  $S$  versus  $D_s$  distribution for the Auger data with that of our simulations. The upper circles connected with dashed/dot-dashed lines represent the mean values of  $S_{\text{sim}}$  of simulated events as in Figure 4, but this time both cases of  $\gamma = 2.7$  and  $2.4$  are presented. The lower circles connected with solid/dotted lines represent the median values of  $S_{\text{sim}}$ . The difference between the cases of  $\gamma = 2.7$  and  $2.4$  is indeed small. The median value of  $S_{\text{sim}}$  for all the simulated events is  $\tilde{S}_{\text{sim}} = 2.80^\circ$ ,  $3.19^\circ$ , and  $3.43^\circ$  for  $\gamma = 2.7$  in Models A, B, and C, respectively. Asterisks denote the Auger events. The mean separation angle for the Auger events is  $\langle S_{\text{Auger}} \rangle = 3.23^\circ$  for 26 events, excluding one event with large  $S$  ( $\approx 27^\circ$ ), while  $\langle S_{\text{Auger}} \rangle = 4.13^\circ$  for all the 27 events. We note that  $\langle S_{\text{Auger}} \rangle \sim \langle S_{\text{sim}} \rangle$ , even though the mean deflection angle is much larger than the mean separation angle in our simulations, that is,  $\langle \theta \rangle \gg \langle S_{\text{sim}} \rangle$ . In all the models, about a half of the Auger events lie within the quartile marks: 15, 13, and 13 events for Models A, B, and C, respectively.

With  $\langle \theta \rangle \sim 15^\circ$  in our simulations, one might naively expect that such large deflection would erase the anisotropy in the arrival direction and the correlation between UHECR events and AGNs (or the LSS of the universe). However, we argue that the large deflection does not necessarily lead to the general isotropy of UHECR arrival direction, if the agent of deflection, the IGMF, traces the local LSS. Suppose that UHECRs are ejected from sources inside the Local Supercluster. Some of them will fly along the Supergalactic plane and arrive

at the Earth; their trajectories would be deflected by the magnetic field between sources and us, but the arrival directions still point toward the Supergalactic plane. Others may be deflected into void regions, and then they will have less chance to get reflected back to the direction toward us due to lack of the turbulent IGMF there. In a simplified picture, we may regard the irregularities in the IGMF as the ‘scatters’ of UHECRs; then the last scattering point will be the arrival direction of UHECRs (see Kotera & Lemoine 2009, for a description of deflection of UHECRs based on this picture). As a result, even with large deflection, we still see more UHECRs from the LSS of clusters, groups, and filaments, and fewer UHECRs from void regions where both sources and scatters are underpopulated. Consequently, the anisotropy in the arrival direction of UHECRs can be maintained and the arrival direction still follows the LSS of the universe.

Below the GZK energy, the proton horizon reaches out to a few Gpc, so the source distribution should look more or less isotropic and the arrival directions should not show a correlation with nearby AGNs. Thus, we do not expect to see anisotropy and correlation for UHECRs with such energy.

In Section 2.4, we showed that the degree of clustering of our model AGNs is similar to that of AGNs from the VCV catalog; the mean of the angular distance  $Q$  between a given AGN to its nearest neighboring AGN is similar,  $\langle Q_{AGN} \rangle \sim \langle Q_{VCV} \rangle$ . In both cases, AGNs follow the matter distribution in the LSS, highly structured and clustered. We point that if along with the reference objects, the CR sources and the IGMF also follow the matter distribution, with  $\langle \theta \rangle \gg \langle S \rangle$ ,  $\langle S \rangle \sim \langle Q \rangle$  is expected. The result that  $\langle S_{Auger} \rangle \sim \langle S_{sim} \rangle \sim \langle Q_{AGN} \rangle \sim \langle Q_{VCV} \rangle$  is indeed consistent with such expectation. This means, however, that the statistics of  $S$  reflect mainly on the distribution of reference objects, rather than the deflection angle.

To further compare the Auger data with our simulations, we plot the cumulative fraction of events,  $F(\leq \log S)$ , versus  $\log S$  for the simulated events (lines) and the Auger events (open circles) in Figure 6. The solid and dotted lines are for the cases of  $\gamma = 2.7$  and 2.4, respectively, and the difference between the two cases is again small. The Kolmogorov-Smirnov (K-S) test yields the maximum difference of  $D = 0.17$ , 0.23, and 0.26 between the Auger data and the simulation data ( $\gamma = 2.7$ ) in Models A, B, and C, respectively; the significance level of the null hypothesis that the two distributions are statistically identical is  $P \sim 0.37$ , 0.09, and 0.04 for Models A, B, and C, respectively. So the null hypothesis that the two distributions for our simulated events and the Auger events are statistically identical cannot be rejected, especially for Model A. This would be a justification for our models of the IGMF, sources of UHECRs, and reference objects. Also we see that Model A with more sources is preferred over Models B and C with fewer sources. But this does not

necessary mean that all the AGNs would be the actual sources of UHECRs. We note that the number of the Auger events used, 27, is still limited. In addition, we consider only UHE protons in this paper. Hence, before we argue the above statements for sure, we will need more observational events and need to know the composition of UHECRs (see Summary and Discussion for further discussion on composition).

### 3.4. Probability of Finding True Sources

With  $\langle\theta\rangle \gg \langle S_{\text{sim}}\rangle$ , there is a good chance that the AGNs found closest to the direction of UHECRs are not the actual sources of UHECRs. To illustrate this point, we first show the distribution of  $D_S$  versus  $D_\theta$  in Figure 7. For some events, the closest AGNs are the actual sources. They are represented by the diagonal line. Around the diagonal line, a noticeable fraction of events are found. Those are the events for which the closest AGNs are found around the true sources; both sources and close-by AGNs are clustered as a part of the LSS of the universe. For the events away from the diagonal line, it is more likely that  $D_S > D_\theta$ . It is because there are more AGNs with larger  $D_S$ ; away from true sources, observed events are more likely to pick up closest AGNs with larger  $D_S$ .

To quantify the consequence of  $\langle\theta\rangle \gg \langle S_{\text{sim}}\rangle$ , we calculated the fraction of true identification,  $f$ , as the ratio of the number of events for which nearest AGNs are their true sources to the total number of simulated events. This is a measure of the probability to find the true sources of UHECRs, when nearest candidates are blindly chosen (which is the best we can do with observed data). In Figure 8, we show the fraction as a function of separation angle,  $S$ . The fraction is largest in Model A with largest  $N_{\text{src}}$ , and smallest in Model C with smallest  $N_{\text{src}}$ . At  $S \sim 2^\circ$  the fraction is about 50 % for Model A, close to 40 % for Model B, and a little above 30 % for Model C, but only 20 – 30 % at  $S = 3^\circ - 4^\circ$ . As the separation angle increases, the fraction decreases gradually to  $\sim 10$  %, indicating lower probabilities to find true sources at larger separation angles. On average, we should expect that in less than 1 out of 3 events, the true sources of UHECRs can be identified, if our model for the IGMF is valid and UHECRs are protons.

## 4. Summary and Discussion

In the search for the nature and origin of UHECRs, understanding the propagation of charged particles through the magnetized LSS of the universe is important. At present, the details of the IGMF are still uncertain, mainly due to limited available information from

observation. Here, we adopted a realistic model universe that was described by simulations of cosmological structure formation; our simulated universe represents the LSS, which is dominated by the cosmic web of filaments interconnecting clusters and groups. The distribution of the IGMF in the LSS of the universe was obtained with a physically motivated model based on turbulence dynamo (Ryu et al. 2008).

To investigate the effects of the IGMF on the arrival direction of UHECRs, we further adopted the following models. Virtual observers of about 1400 were placed at groups of galaxies, which represent statistically the Local Group in the simulated model universe. Then, we set up a set of about 500 AGN-like “reference objects” within 75 Mpc from each observer, at clusters of galaxies (deep gravitational potential wells) along the LSS. They represent a class of astronomical objects with which we performed a correlation analysis for simulated UHECR events. We considered three models, in which subsets of the reference objects were selected as AGN-like sources of UHECRs (see Table 1). UHE protons of  $E \geq 60$  EeV with power-low energy spectrum were injected at those sources, and the trajectories of UHE protons in the magnetized cosmic web were followed. At observer locations, the events with  $E \geq 60$  EeV from sources within a sphere of radius 75 Mpc were recorded and analyzed.

To characterize the clustering of the reference objects, we calculated the angular distance,  $Q$ , from a given reference object to its nearest neighbor. The mean value for our model AGNs in the simulated universe is  $\langle Q_{\text{AGN}} \rangle = 3.68^\circ \pm 1.66^\circ$ , while that for 442 AGNs from the VCV catalog is  $\langle Q_{\text{VCV}} \rangle = 3.55^\circ$ . This demonstrates that the two samples have a similar degree of clustering and are highly structured (e.g.  $\langle Q_{\text{iso}} \rangle \approx 11^\circ$  for the isotropic distribution).

With our model IGMF, the deflection angle,  $\theta$ , between the arrival direction of UHE protons and the sky position of their actual sources, is quite large with the mean  $\langle \theta \rangle \sim 14 - 17.5^\circ$  and the median  $\tilde{\theta} \sim 7 - 10^\circ$ , depending on models with different numbers of sources (see Table 1). On the other hand, the separation angle between the arrival direction and the sky position of nearest reference objects is substantially smaller with the mean  $\langle S_{\text{sim}} \rangle \sim 3.5 - 4^\circ$  and the median  $\tilde{S}_{\text{sim}} = 2.8 - 3.5^\circ$ . That is, we found that while  $\langle \theta \rangle \sim 4 \langle S_{\text{sim}} \rangle$ ,  $\langle S_{\text{sim}} \rangle$  is similar to  $\langle Q_{\text{AGN}} \rangle$ . For the Auger events of highest energies in Abraham et al. (2008a), with 442 nearby AGNs from the VCV catalog as the reference objects, the mean separation angle is  $\langle S_{\text{Auger}} \rangle = 3.23^\circ$  for the 26 events, excluding one event with large  $S$  ( $\approx 27^\circ$ ), while  $\langle S_{\text{Auger}} \rangle = 4.13^\circ$  for all the 27 events. Hence,  $\langle S_{\text{Auger}} \rangle \sim \langle Q_{\text{VCV}} \rangle \sim \langle S_{\text{sim}} \rangle \sim \langle Q_{\text{AGN}} \rangle$ . This implies that the separation angle from the Auger data would be determined primarily by the distribution of reference objects (AGNs), and may not represent the true deflection angle.

We further tested whether the distributions of separation angle,  $S$ , for our simulated events and for the Auger events are statistically comparable to each other. According the

Kolmogorov-Smirnov test for the cumulative fraction of events,  $F(\leq \log S)$ , versus  $\log S$ , the significance level of the null hypothesis that the two distributions are drawn from the identical population is as large as  $P \sim 0.37$  for Model A (see Table 1). Thus, we argued that our simulation data, especially in Model A, are in a fair agreement with the Auger data. This test also showed that the model with more sources (Model A) is preferred over the models with fewer sources (Models B and C).

The fact that  $\langle \theta \rangle \gg \langle S_{\text{sim}} \rangle$  implies that the AGNs found closest to the direction of UHECRs may not be the true sources of UHECRs. We estimated the probability of finding the true sources of UHECRs, when nearest reference objects are blindly chosen:  $f(S)$  is the ratio of the number of true source identifications to the total number of simulated events. This probability is  $\sim 50 - 30\%$  at  $S \sim 2^\circ$ , but decreases to  $\sim 10\%$  at larger separation angle. On average, in less than 1 out of 3 events, the true sources of UHECRs can be identified in our simulations, when nearest reference objects are chosen.

The distribution of  $\theta$  versus  $D_\theta$  shows a bimodal pattern in which  $\theta$  is on average larger either for nearby sources (for  $D_\theta \lesssim 15$  Mpc) or for distant sources (for  $D_\theta \gtrsim 30$  Mpc) with the minimum at the intermediate distance of  $D_{\theta, \text{min}} \sim 20 - 30$  Mpc. The distribution of  $S$  versus  $D_s$  shows a similar, but weaker sign of the bimodal pattern. This behavior is a characteristic signature of the magnetized cosmic web of the universe, where filaments are the most dominant structure. When a large number of super-GZK events are accumulated, we may find the signature of the cosmic web of filaments in the  $S$  versus  $D_s$  distribution.

Finally, we address the limitations of our work. (1) We worked in a simulated universe with specific models for the elements such as the IGMF, observers, sources, and reference objects, but not in the real universe. So we could make only statistical statements. (2) It has been shown previously that adopting different models for the IGMF, very different deflection angles are obtained (see Sigl et al. 2003; Dolag et al. 2005; Das et al. 2008). We argue that our model for the IGMF is most plausible, since it is a physically motivated model based on turbulence dynamo without involving an arbitrary normalization (Ryu et al. 2008). Nevertheless, our IGMF model should be confirmed further by observation. (3) The sources of UHECRs may not be objects like AGNs, but could be objects extinguished a while ago, such as gamma-ray bursts (see, e.g., Vietri 1995; Waxman 1995), or sources spread over space like cosmological shocks (see, e.g., Kang et al. 1996; Kang et al. 1997). The injection energy spectrum of power-law with cut-off at an arbitrary maximum energy (see Section 2.6) would be unrealistic. The IGMF in the Local Group (see Paper I), although currently little is known, might be strong enough to substantially deflect the trajectories of UHECRs. All of those will have effects on the quantitative results, which should be investigated further. (4) Recently, the Auger collaboration disclosed the analysis, which suggests a substantial fraction



of highest energy UHECRs might be iron nuclei (Unger et al. 2007; Wahberg et al. 2009). This is in contradiction with the analysis of the HiRes data, which indicates highest energy UHECRs would be mostly protons (Sokolsky & Thomson 2007). The issue of composition still needs to be settled down among experiments. Iron nuclei, on the way from sources to us, suffer much larger deflection than protons. Hence, if a substantial fraction of UHECRs is iron, some of our findings will change, a question which should be investigated in the future.

The authors would like to thank P. L. Biermann for stimulating discussion. The work was supported by the Korea Research Foundation (KRF-2007-341-C00020) and the Korea Foundation for International Cooperation of Science and Technology (K20702020016-07E0200-01610).

## REFERENCES

- Abbasi, R. U. et al. (HiRes Collaboration) 2004, *ApJ*, 610, L73
- Abbasi, R. U. et al. (HiRes Collaboration) 2006, *ApJ*, 636, 680
- Abbasi, R. U. et al. (HiRes Collaboration) 2008a, *Phys. Rev. Lett.*, 100, 101101
- Abbasi, R. U. et al. (HiRes Collaboration) 2008b, *Astropart. Phys.*, 30, 175
- Abbasi, R. U. et al. (HiRes Collaboration) 2009, *Proc. of 31st Int. Cosmic Ray Conf. (Lodz, Poland)*
- Abraham, J. et al. (Auger Collaboration) 2008a, *Astropart. Phys.*, 29, 188
- Abraham, J. et al. (Auger Collaboration) 2008b, *Phys. Rev. Lett.*, 101, 061101
- Aublin, J. et al. (Auger Collaboration) 2009, *Proc. of 31st Int. Cosmic Ray Conf. (Lodz, Poland)*
- Berezinsky, V. 2009, *Nucl. Phys. B (Proc. Suppl.)*, 188, 227
- Berezinsky, V., Gazizov, A., & Grigor'eva, S. I. 2006, *Phys. Rev. D*, 74, 043005
- Berezinsky, V. & Grigor'eva, S. I. 1988, *A&A*, 199, 1
- Biermann, L. 1950, *Z. Naturforsch, A*, 5, 65
- Biermann, P. L. & Strittmatter, P. A. 1987, *ApJ*, 322, 643

- Bird, D. J. et al. (Fly's Eye Collaboration), 1994, *ApJ*, 424, 491
- Cho, J. & Ryu, D. 2009, *ApJ*, in press (arXiv:0908.0610)
- Das, S., Kang, H., Ryu, D. & Cho, J. 2008, *ApJ*, 682, 29 (Paper I)
- Dolag, K., Grasso, D., Springel, D., & Tkachev, I. 2005, *J. Cosmology Astropart. Phys.*, 1, 009
- Egorova V. P. et al. (Yakutsk Collaboration) 2004, *Nucl. Phys. B (Proc. Suppl.)*, 136, 3
- Greisen, K. 1966, *Phys. Rev. Lett.*, 16, 748
- Hague, J. D. et al. (Auger Collaboration) 2009, *Proc. of 31st Int. Cosmic Ray Conf. (Lodz, Poland)*
- Hayashida, N. et al. (AGASA Collaboration) 1996, *Phys. Rev. Lett.*, 77, 1000
- Hillas, A. M. 2009, submitted to *Astropart. Phys.* (arXiv:0906.0280)
- Kang, H., Rachen, J. P., & Biermann, P. L. 1997, *MNRAS*, 286, 25
- Kang, H., Ryu, D., & Jones, T. 1996, *ApJ*, 456, 422
- Karachentsev, I. D., Karachentseva, V. E., Huchtmeier, W. K., & Makarov, D. I. 2004, *AJ*, 127, 2031
- Kotera, K. & Lemoine, M. 2009, *Phys. Rev. D*, 77, 123003
- Kronberg, P. P., Dufton, Q. W., Li, H., & Colgate, S. A. 2001, *ApJ*, 560, 178
- Kulsrud, R. M., Cen, R., Ostriker, J. P., & Ryu, D. 1997, *ApJ*, 480, 481
- Nagano, A. & Watson, A. A. 2000, *Rev. Mod. Phys.*, 72, 689
- Puget, J. L., Stecker, F. W., & Bredekamp, J. H. 1976, *ApJ*, 205, 638
- Rasmussen, J. & Pedersen, K. 2001, *ApJ*, 559, 892
- Ryu, D., Kang, H., & Biermann, P. L. 1998, *A&A*, 335, 19
- Ryu, D., Kang, H., Cho, J., & Das, S. 2007, *Science*, 320, 909
- Ryu, D., Kang, & Das, S. 2009, *Proc. of 31st Int. Cosmic Ray Conf. (Lodz, Poland)*
- Ryu, D., Ostriker, J. P., Kang, H., & Cen, R. 1993, *ApJ*, 414, 1

- Schüssler, K. et al. (Auger Collaboration) 2009, Proc. of 31st Int. Cosmic Ray Conf. (Lodz, Poland)
- Shinozaki K. & Teshima M. (AGASA Collaboration) 2004, Nucl. Phys. B (Proc. Suppl.), 136, 18
- Sigl, G., Miniati, F., & Ensslin, T. A. 2003, Phys. Rev. D, 68, 043002
- Sokolsky, P. & Thomson, G. 2007, J. Phys. G, 34, R401
- Stanev, T. 1997, ApJ, 479, 290
- Takami, H., Nishimichi, T., & Sato, K. 2009, submitted to J. Cosmology Astropart. Phys.(arXiv:0910.2765)
- Takami, H. & Sato, K. 2008, ApJ, 681, 1279
- Takeda, M. et al. (AGASA Collaboration) 1999, ApJ, 522, 225
- The Pierre Auger Collaboration, 2007, Science, 318, 939
- Unger, M. et al. (Auger Collaboration) 2007, Proc. of 30st Int. Cosmic Ray Conf. (Mérida, Mexico)
- Véron-Cetty, M. P. & Véron, P. 2006, A&A, 455, 773 (VCV)
- Vietri, M. 1995, ApJ, 453, 883.
- Wahlberg, H. et al. (Auger Collaboration) 2009, Proc. of 31st Int. Cosmic Ray Conf. (Lodz, Poland)
- Watson, A. A. 2006, Nucl. Phys. Proc. Suppl., 151, 83
- Waxman, E. 1995, Phys. Rev. Lett., 75, 386
- Xu, Y., Kronberg, P. P., Habib, S., & Dufton, Q. W. 2006, ApJ, 637, 19
- Zatsepin, G. T. & Kuz'min, V. A. 1966, JETP Lett., 4, 78

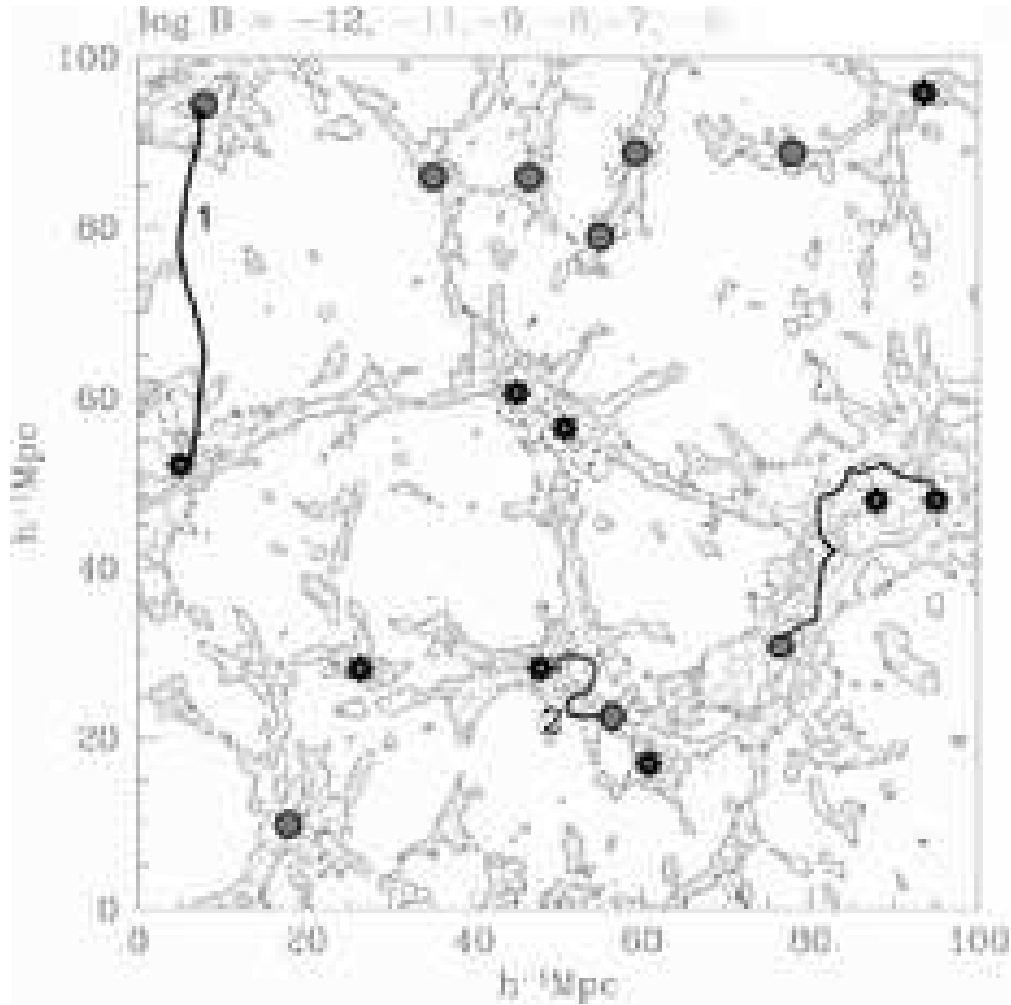


Fig. 1.— Distribution of the IGMF in a two-dimensional slice of  $(143 \text{ Mpc})^2$  in the simulated universe. Locations of virtual observers (circles) and model AGNs (stars) are schematically marked at clusters and groups of galaxies. Paths of UHECRs from sources to observers are also schematically drawn.

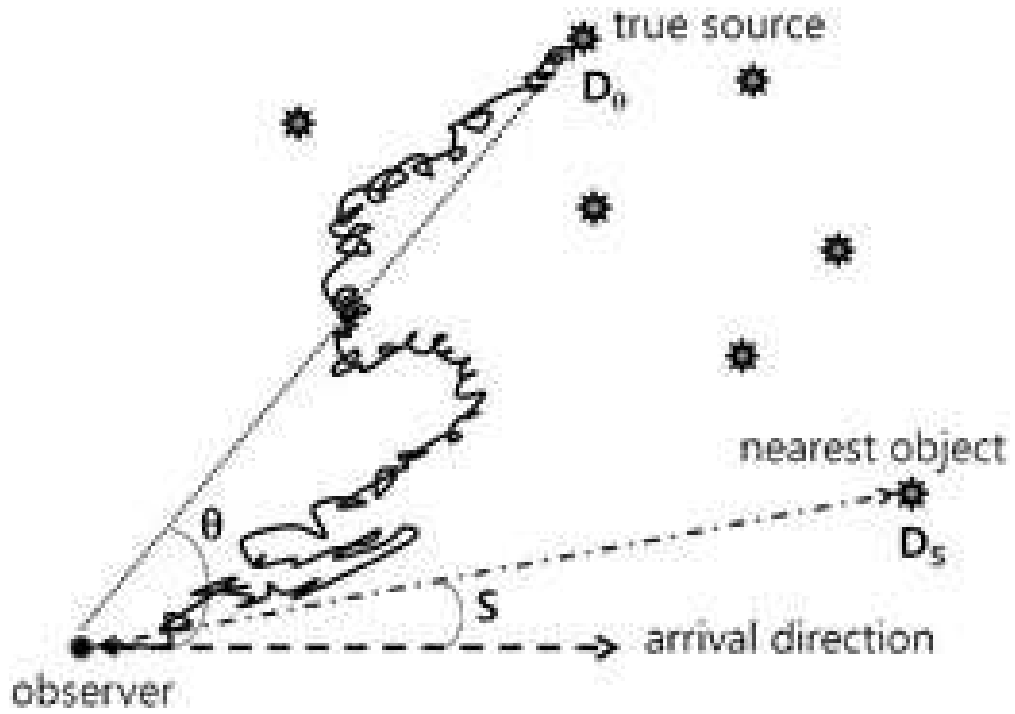


Fig. 2.— Geometry of the deflection angle,  $\theta$ , the separation angle,  $S$ , the distance to the true source,  $D_\theta$ , and the distance to the nearest object,  $D_S$ . The path of the UHECR event from the source to observer is schematically drawn.

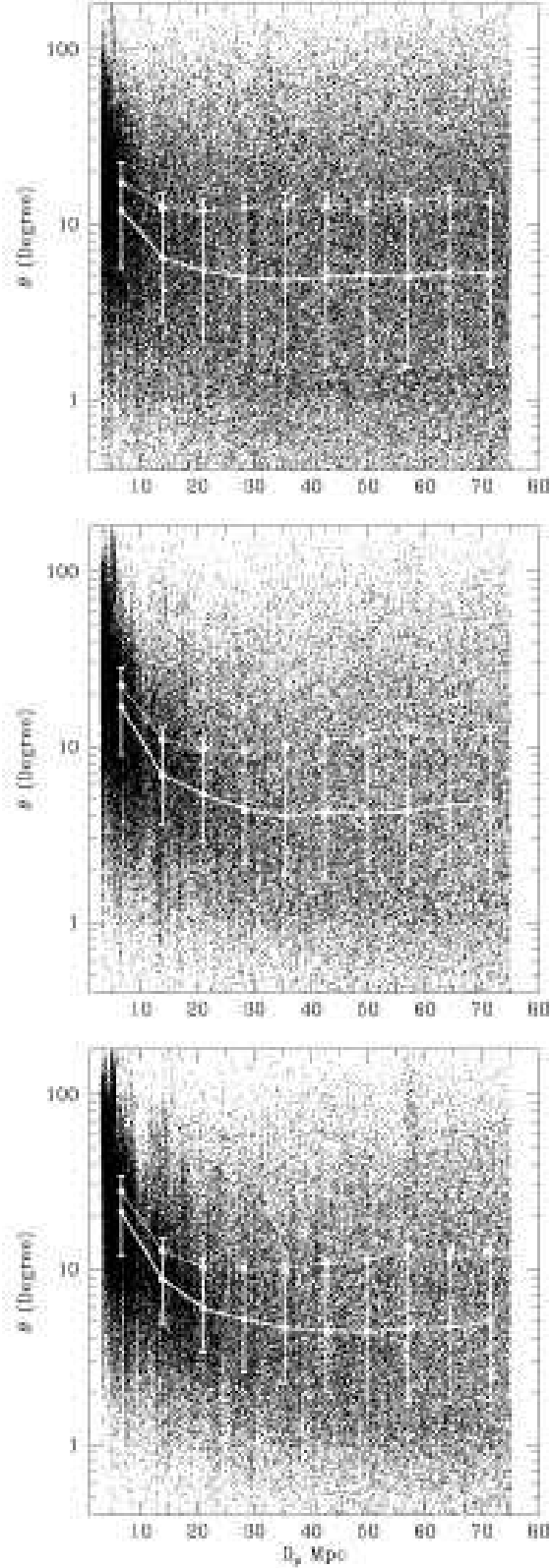


Fig. 3.— Distribution of deflection angles ( $\theta$ ) as a function of distance to true sources ( $D_\theta$ ). Dots represent UHE proton events recorded in our simulations. Circles connected with dotted lines (upper) and solid lines (lower) show the mean and median values, respectively. Vertical lines connect the marks of first and third quartiles in given  $D_\theta$  bins. Top, middle, and bottom panels are for Model A, Model B, and Model C, respectively. The cases of  $\gamma = 2.7$  are shown.

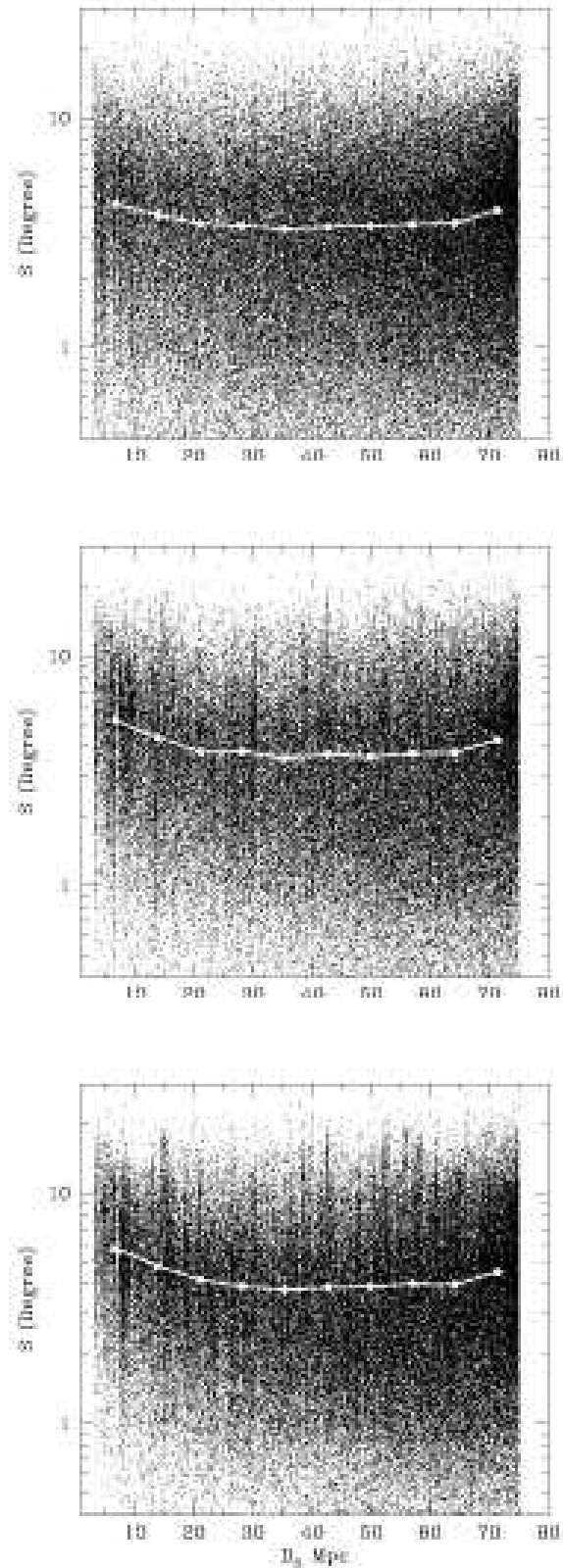


Fig. 4.— Distribution of separation angles between the directions of UHE protons and nearest model AGNs ( $S$ ) as a function of distance to nearest model AGNs ( $D_S$ ). Dots represent UHE proton events recorded in our simulations. Circles connected with solid lines show the mean values. Top, middle, and bottom panels are for Model A, Model B, and Model C, respectively. The cases of injection spectral index  $\gamma = 2.7$  are shown.

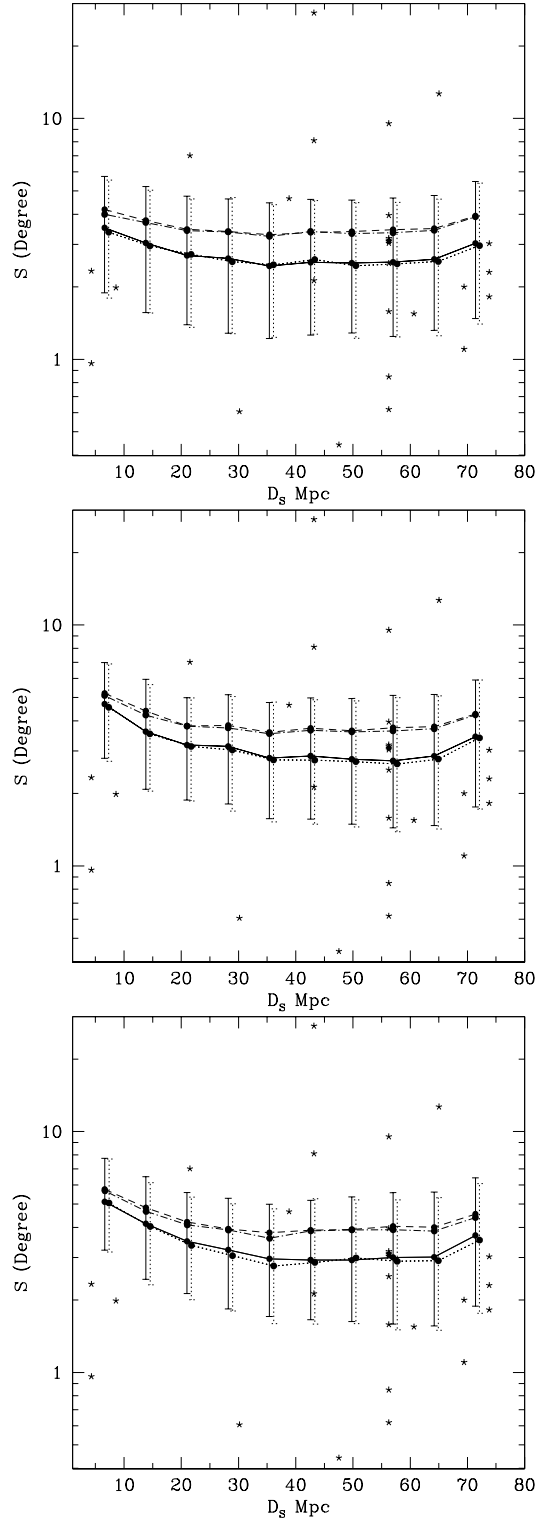


Fig. 5.— Mean (upper circles) and median (lower circles) values of  $S$  as a function of  $D_S$  for UHE proton events in our simulations. Vertical lines connect the marks of first and third quartiles in given  $D_S$  bins. Circles connected with dashed lines (upper) and solid lines (lower) are for  $\gamma = 2.7$ , and those connected with dot-dashed lines (upper) and dotted lines (lower) are for  $\gamma = 2.4$ . The mean  $S$  for  $\gamma = 2.7$  are the same as those in Figure 2. The median and quartiles for  $\gamma = 2.4$  are horizontally shifted for better visibility. Asterisks denote  $S$  for the 27 Auger events of highest energies, published in Abraham et al. (2008a), with nearby AGNs from the VCV catalog. Top, middle, and bottom panels are for Model A, Model B, and Model C, respectively.



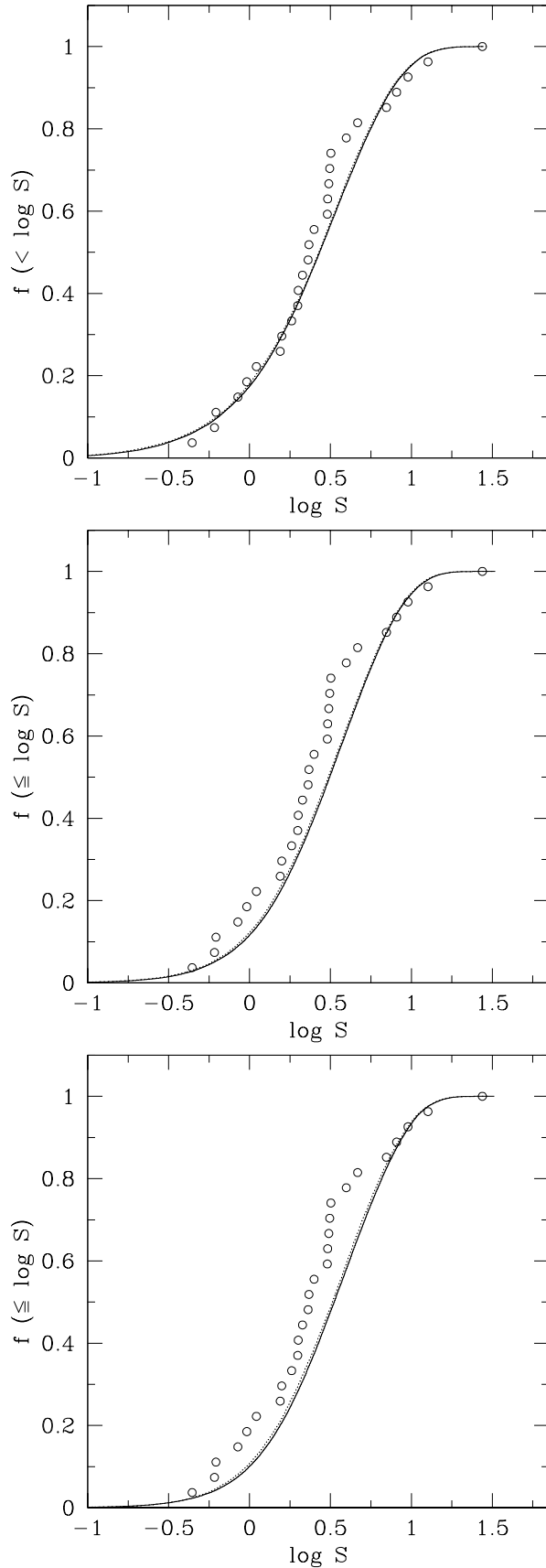


Fig. 6.— Cumulative fraction of UHECR events with separation angle smaller than  $S$ . Solid and dotted lines denote the results calculated with the UHE proton events in our simulations for  $\gamma = 2.7$  and  $2.4$ , respectively. Top, middle, and bottom panels are for Model A, Model B, and Model C, respectively. Open circles denote the result for the 27 Auger

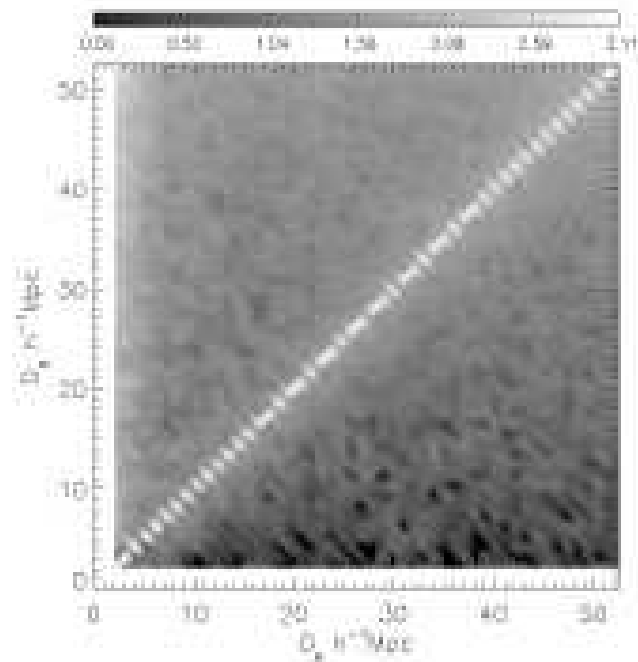


Fig. 7.— Distance to nearest model AGNs,  $D_S$ , versus distance to true sources,  $D_\theta$ , for the UHECR events in Model A. The case of  $\gamma = 2.7$  is shown. Color codes the number of events in  $\log_{10}$  scale in bins of  $\Delta D_\theta \times \Delta D_S$ . The maximum distance is 75 Mpc for both  $D_S$  and  $D_\theta$ .

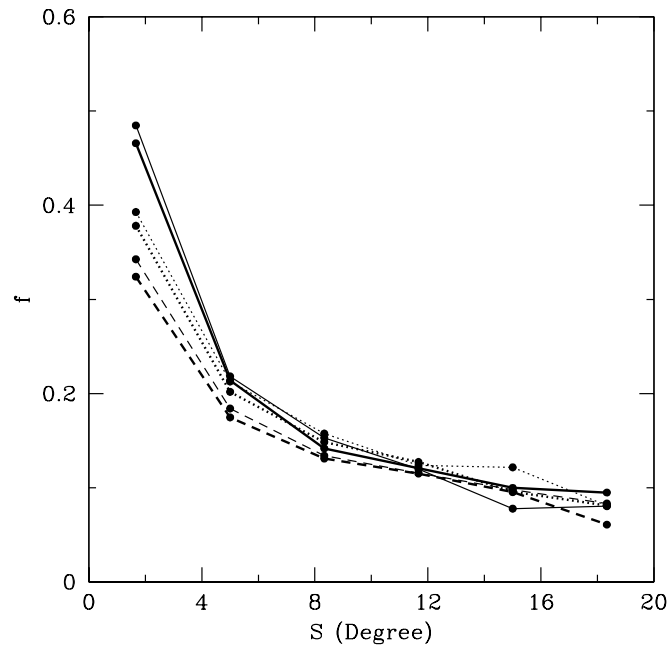


Fig. 8.— Fraction ( $f$ ) of UHE proton events recorded in our simulations, for which their true sources are identified as closest AGNs in the sky, as a function of  $S$ . Dashed, dotted, and solid lines are for Model A, Model B, and Model C, respectively. Heavy and light lines denote the fractions for  $\gamma = 2.7$  and  $2.4$ , respectively.